

Variable Star Classification Using Multi-View Metric Learning

K. B. Johnston^{1,5} S.M. Caballero-Nieves,¹ V. Petit,² A.M. Peter,³ and R. Haber,⁴

¹ Aerospace, Physics and Space Sciences Dept., Florida Institute of Technology, 150 W. University Blvd., Melbourne, FL, US
e-mail: kyjohnst2000@my.fit.edu

² Physics and Astronomy Dept., University of Delaware, Newark, DE, USA,

³ Computer Engineering and Sciences Dept., Florida Institute of Technology, 150 W. University Blvd., Melbourne, FL, US

⁴ Mathematical Sciences Dept., Florida Institute of Technology, 150 W. University Blvd., Melbourne, FL, US

⁵ Defense Group Melbourne, Perspecta Inc., 4849 N. Wickham Rd., Melbourne, FL, USA

November 8, 2021

ABSTRACT

Context. Comprehensive observations of variable stars can include time domain photometry in a multitude of filters, spectroscopy, estimates of color (e.g. U-B), etc. When the objective is to classify variable stars, traditional machine learning techniques distill these various representations (or views) into a single feature vector and attempt to discriminate among desired categories.

Aims. In this work, we propose an alternative approach that inherently leverages multiple views of the same variable star.

Methods. Our multi-view metric learning framework enables robust characterization of star categories by directly learning to discriminate in a multi-faceted feature space, thus, eliminating the need to combine feature representations prior to fitting the machine learning model. We also demonstrate how to extend standard multi-view learning, which employs multiple vectorized views, to the matrix-variate case which allows very novel variable star signature representations.

Results. The performance of our proposed methods is evaluated on the UCR Starlight and LINEAR datasets. Both the vector and matrix-variate versions of our multi-view learning framework perform favorably — demonstrating the ability to discriminate variable star categories..

Key words. methods: data analysis – methods: statistical – techniques: photometric

1. Introduction

The classification of variable stars relies on the proper selection of tell-tale light-curve signatures representing a specific variability type (referred to as the features of interest in machine learning terminology) and an automated detection/separation framework that can differentiate different variable stars (referred to as the classifier in machine learning terminology).

Classically, the astroinformatics-community standard features include: the quantification of statistics associated with the time domain photometric data (e.g., mean, standard deviation, kurtosis), Fourier decomposition of the data (e.g., ratio of frequency, peak frequency), and color information in both the optical and infrared domain (Nun et al. 2015; Miller et al. 2015).

Likewise, standard classification techniques in the astroinformatics-community span a few areas: (i) the classifier is designed such that the user selects features and the classifier is trained on variables with a known type ("expert selected features, for correlation discovery", Debosscher 2009; Sesar et al. 2011; Richards et al. 2012; Graham et al. 2013a; Armstrong et al. 2016; Mahabal et al. 2017; Hinners et al. 2018),

(ii) the classifier is designed such that the computer selects the optimal features and the classifier is trained on variables with a known type (McWhirter et al. 2017; Naul et al. 2018, "computer selected features, for correlation discovery"),

(iii) the classifier (clustering algorithm) is designed such that that user selects features and variables with an unknown type are provided ("expert selected features, for class discovery", Valenzuela and Pichara 2018; Modak et al. 2018).

These efforts have been hampered by multiple factors. First, the underlying foundational data to be used in classification is biased either resulting from the original composition of the survey from which the training data is selected (Angeloni et al. 2014) or the choice of building a training set containing only a subset of the top five to ten most frequent class-types Kim and Bailer-Jones (2016); Pashchenko et al. (2018); Naul et al. (2018). In our research, no efforts were found in the literature that address all variables identified by Samus' et al. (2017)—most address some subset.

Second, the development of expertly selected feature sets is often keyed to the original selection of variable stars of interest, and their definition. As surveys become more complete and more dense in observations, the complexity of the problem is likely to grow as a result of further refinement of classification definitions (Samus' et al. 2017).

Third, the legacy expertly selected features (Richards et al. 2011) are often co-linear, resulting in little to no new information or separability despite the increase in dimensionality and additional increase in computational power needed to manage the data (D'Isanto et al. 2016). Lastly, increases in feature dimensionality (with co-linear data) results in needlessly increasing the sparsity of the training data space (e.g., curse of dimensionality). This requires increasingly more complex classifier designs to both support the dimensionality as well as the potential non-linear class-space separation.

Presented here is a methodology that addresses these issues using a combination of new features and advanced classifiers designs.

Two novel transforms, Slotted Symbolic Markov Model (SSMM, Johnston and Peter 2017) and Distribution Fields (DF, Johnston et al. 2019), are used to generate viable feature spaces for the classification of variable stars. SSMM requires no phasing of the time domain data but still provides a feature that is shape based, DF allows for the consideration of the whole phased waveform without additional picking and choosing of metrics from the waveform (i.e., see Helfer et al. 2015). Both of these transforms require only processed (artifact removed) time domain data, i.e. light curves.

Each of these new transforms quantify the light curve shape, using either phased and un-phased data. This methodology of quantifying all available time domain information within the transformations identified and allowing the selected classifier to optimize the features of interests, contrasts with the traditional methodology of using un-optimized, biased, sub-selected features that may—or may not—contain information that is vital to the discrimination of different types of variable stars.

However, the features we selected are matrix-variate (i.e. $\mathbb{R}^{m \times n}$), thus to accommodate the usage of either of these features (or both) we introduce two classifiers to the astroinformatics community. The first, Large Margin Multi-view Metric Learning (LM³L, Hu et al. 2014) relies on dimensionality reduction methodologies. The second, Large Margin Multi-view Metric Learning with Matrix Variates (LM³L-MV), is a novel development and inherently generates compact feature spaces as part of the optimization process. Both classifiers allow for the usage of multiple domains in the classification process (both SSMM and DF simultaneously).

Multi-view learning is a methodology that can provide a major benefit to the astronomical community. Astronomy often deals with multiple transformations (e.g., Fourier Domain, Wavelet Domain, statistical...etc) and multiple domains of data types (visual, radio frequency, high energy, particle, etc.). The ability to handle, and just as importantly co-train an optimization algorithm on, multiple domain data will be necessary as the multitude of data grows. Furthermore, metric learning decisions have an implicit traceability: the ability to follow from the classifier’s decision, to the weights associated with each individual feature used as part of the classification, to the nearest-neighbors used in making the decision provide a clear idea of why the classifier made the decision. This direct comparison of newly observed with prior observations, and the justification via historical comparison, make this method ideal for astronomical—and indeed scientific—applications.

This paper additionally outlines a system design that allows for the tools provided here to be translated to many different scenarios, using many different input values, providing interested scientists flexibility of use. In this paper will be organized as follows: (1) summarize current stellar variable classification efforts, features currently in use, and machine learning methodologies exercised (2) review the features used (statistics, color, DF and SSMM) (3) review the classification methodologies used (metric learning, LM³L, and LM³L-MV) (4) demonstrate our optimization of feature extraction algorithm for our datasets, leveraging “simple” classification methods (k-NN) and cross-validation processes (5) demonstrate our optimization of classification parameters for LM³L and LM³L-MV via cross-validation and (6) report on the performance of the feature/classifier pairing. Our proposal is an implementation of both the feature extraction and classifier for the purposes of multi-class identification, that can

handle raw observed data. The project software is provided publicly at the associated GitHub repository ¹

2. Theory and Design

We present an initial set of time domain feature extraction methods; the design demonstrated is modular in nature, allowing for a user to append or substitute feature spaces that an expert has found to be of utility in the identification of variable stars. Although our initial goal is variable star identification, given a separate set of features this method could be applied to other astroinformatics problems (i.e., image classification for galaxies, spectral identification for stars or comets, etc.). While we demonstrate the classifier has a multi-class classification design, which is common in the astroinformatics references we have provided, the design here can easily be transformed into a one-vs-all design (Johnston and Oluseyi 2017) for the purposes of generating a detector or classifier designed specifically to a user’s needs (Johnston et al. 2019).

2.1. Signal Conditioning

Required are features that can respond to the various signal structures that are unique to the classes of interest, i.e. phased light shape, frequency distribution, phase distribution, etc.). Our implementation starts with raw data (such as astronomical light curves) as primary input, which are then mapped into a specific feature space. To support these transformations, a set of signal conditioning methods are implemented for the two new feature space presented below. These techniques are based on the methods presented in Johnston and Peter (2017) and are fairly common in the industry. The data that is leveraged—with respect to classification of the waveform—is on the order of hundreds of observations over multiple cycles. While the data is not cleaned as part of the upfront process, the features that are implemented are robust enough to not be affected by intermittent noise. The raw waveform is left relatively unaffected, however smoothing does occur on the phased waveform to generate a new feature vector, i.e. a phased smoothed waveform.

The phased waveform is generated via folding the raw waveform about a period found to best represent the cyclical process (Graham et al. 2013b). The SUPER-SMOOTHER algorithm (Friedman 1984) is used to smooth the phased data into a functional representation. Additionally in some cases, the originating survey/mission will perform some of these signal conditioning processes as part of their analysis pipeline (e.g., Kepler). This includes outlier removal, period finding, and long term trend removal. Most major surveys include a processing pipeline, our modular analysis methods provide a degree of flexibility that allow the implementer to take advantage of these pre-applied processes. Specifically of use, while our feature extraction SSMM does not require a phased waveform, the DF feature does, thus period finding methods are of importance.

Most of the period finding algorithms are methods of spectral transformation with an associated peak/max/min finding algorithm and include such methods as: discrete Fourier transform, wavelets decomposition, least squares approximations, string length, auto-correlation, conditional entropy and auto-regressive methods. Graham et al. (2013b) review these transformation methods (with respect to period finding), and find that the optimal period finding algorithm is different for different types of variable stars. The Lomb–Scargle method was selected as the

¹ <https://github.com/kjohnston82/VariableStarAnalysis>

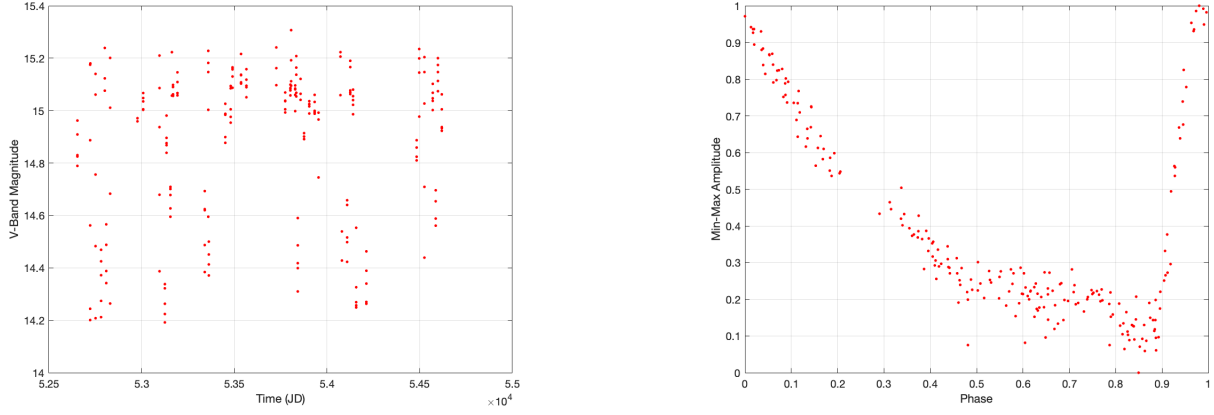


Fig. 1. Left: Raw Time Domain Data, Right: Corresponding Transformed Phased Time Domain Data, Example Given for RR Lyr Type Variable

main method for generating a primary period for this implementation. For more information, our implementation of the Lomb–Scargle algorithm is provided as part of the Variable Star package².

2.2. Feature Extraction

For our investigation we have selected feature spaces that quantify the functional shape of repeated signal—cyclostationary signal—but are dynamic enough to handle impulsive type signals (e.g., supernova) as well. This particular implementation design makes the most intuitive sense, visual inspection of the light curve is how experts identify these sources. Prior research on time domain data identification has varied between generating machine learned features (Bos et al. 2002; Broersen 2009; Blomme et al. 2011; Bolós and Benítez 2014; Gagniac 2017), implementing generic features (e.g. Fourier domain features; Debusscher 2009; Richards et al. 2012; Palaversa et al. 2013; Masci et al. 2014), and looking at shape or functional based features (e.g. DF, SSMM; Park and Cho 2013; Haber et al. 2015).

We implement two novel time domain feature space transforms: SSMM and DF. It is not suggested that these features are going to be the best in all cases, nor are they the only choice as is apparent from Fulcher et al. (2013). Any feature space, so long as it provides separability, would be usable here. One need only think of how to transform the observable (time domain, color, spectra, etc.) into something that is a consistent signature for stars in given class-type (i.e., variable star type).

SSMM itself is an effective feature for discriminating variable star types as shown by Johnston and Peter (2017). Similarly, DF has been shown to be a valuable feature for discriminating time domain signatures, see Helfer et al. (2015) and Johnston et al. (2019).

2.2.1. Slotted Symbolic Markov Models (SSMM)

Slotted Symbolic Markov Models (SSMM) is useful in the differentiation between variable star types (Johnston and Peter 2017). The time domain slotting described in Rehfeld et al. (2011) is used to regularize the sampling of the photometric observations. The resulting regularized sampled waveform is transformed into a state space (Lin et al. 2007; Bass and Borne 2016); thus the result of the conditioning is the stochastic process

$\{y_n, n = 1, 2, \dots\}$. The stochastic process is then used to populate the empty matrix \mathbf{P} (Ge and Smyth 2000)—the elements of \mathbf{P} are populated as the transition state probabilities (equation 1).

$$\mathbf{P}\{y_{n+1} = j | y_n = i, y_{n-1} = i_{n-1}, \dots, y_1 = i_1, y_0 = i_0\} = P_{ij} \quad (1)$$

The populated matrix \mathbf{P} is the SSMM feature; and is often described as a first order Markov Matrix.

2.2.2. Distribution Field (DF)

A distribution field (DF) is an array of probability distributions, where probability at each element is defined as equation 2 (Helfer et al. 2015; Sevilla-Lara and Learned-Miller 2012).

$$DF_{ij} = \frac{\sum_k^N [y_j < f(x_i \leq \phi_k \leq x_{i+1})_N < y_{j-1}]}{\sum_k^N [y_j < f(\phi_k)_N < y_{j-1}]}, \quad (2)$$

where N is the number of samples in the phased data, and $[\]$ is the Iverson bracket (Iverson 1962), given as

$$[P] = \begin{cases} 1 & P = \text{true} \\ 0 & \text{otherwise,} \end{cases} \quad (3)$$

Similarly, $f(\phi_k)$ is the smoothed phased data, and y_j and x_i are the corresponding normalized amplitude and phase bins. The bins are defined as $x_i = 0, 1/n_x, 2/n_x, \dots, 1$ and $y_i = 0, 1/n_y, 2/n_y, \dots, 1$; n_x is the number of time bins, and n_y is the number of amplitude bins. The result is a right stochastic matrix, i.e., the rows sum to 1. Bin number, n_x and n_y , is optimized by cross-validation as part of the classification training process.

2.3. Classification and Metric Learning

The classification methodology known as metric learning has its roots in the understanding of how and why observations are considered similar. The very idea of similarity is based around the numerical measurement of distance, and the computation of a distance is generated via application of a distance function. Bellet et al. (2015) define the metric distance as equation 4

$$d(x, x') = \sqrt{(x - x')^T \mathbf{M} (x - x')}; \quad (4)$$

² fit.astro.vsa.analysis.feature.LombNormalizedPeriodogram

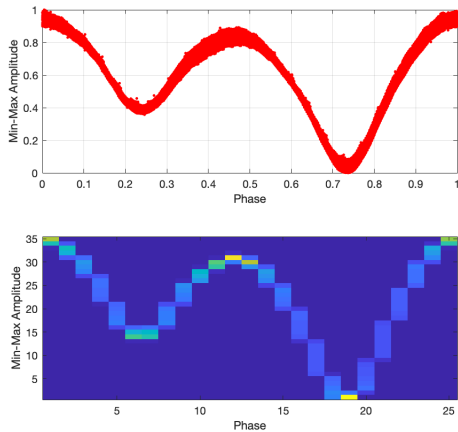


Fig. 2. Folded Time Domain Data Transformed into the DF Feature space, Example Given for Eclipsing Binary Type Variable

where $X \subseteq \mathbb{R}^d$ and the metric is required to be $\mathbf{M} \in \mathbb{S}_+^d$ is the cone of symmetric positive semi-definite (PSD) $d \times d$ real valued matrices. Metric learning seeks to optimize this distance, via manipulation of the metric \mathbf{M} , based on available side data. How the optimization occurs, what is focused on and what is considered important, i.e. the construction of the objective function, is the underlying difference between the various metric learning algorithms.

The side information is defined as the set of labeled data $\{x_i, y_i\}_{i=1}^n$. Furthermore the triplet is defined as (x_i, x_j, x_k) where x_i and x_j have the same label but x_i and x_k do not. It is expected then, based on the definition of similarity and distance, that $d(x_i, x_j) < d(x_i, x_k)$, i.e., that the distances between similar labels is smaller than the distances between dissimilar ones. Methods such as Large Margin Nearest Neighbor (LMNN, Weinberger et al. 2009) use this inequality to defined an objective function that optimizes the metric to bring similar things closer together, while pushing dissimilar things further apart.

Given the metric learning optimization process, the result is a tailored distance metric and associated distance function (equation 4). This distance function is then used in a standard k-NN classification algorithm. The k-NN algorithm estimates a classification label based on the closest samples provided in training (Altman 1992). If x_n is a set of training data n big, then we find the distance between a new pattern x_i and each pattern in the training set. The new pattern is classified depending on the majority of class labels in the closest k data points.

Prior studies have initially addressed the potential of using metric learning as a means for classification of variable stars (Johnston et al. 2019). Metric learning has a number of benefits that are advantageous to the astronomer:

- Metric learning uses nearest neighbors (k-NN) classification to generate the decision space (Hastie et al. 2009; Duda et al. 2012), k-NN provides instant clarity into the reasoning behind the classifiers decision (based on similarity, “ x_i is closer to x_j than x_k ”).
- Metric learning leverages side information (the supervised labels of the training data) to improve the metric, i.e. a transformation of the distance between points that favors a specific goal: similar closer together, different further apart, simplicity of the metric, feature dimensionality reduction, etc.. This side data is based on observed prior analyzed data, thus decisions have a grounding in expert identification as op-

posed to black-box machine learning (Bellet et al. 2015). Dimensionality reduction in particular can be helpful for handling feature spaces that are naturally sparse.

- k-NN can be supported by other algorithm structures such as data partitioning methods to allow for a rapid response time in assigning labels to new observations, despite relying upon a high number of training data (Faloutsos et al. 1994).
- The development of an anomaly detection functionality (Chandola et al. 2009), which has been shown to be necessary to generate meaningful classifications (see: Johnston and Peter 2017; Johnston and Oluseyi 2017), is easily constructed from the k-NN metric learning framework.

2.3.1. Multi-View Learning

We address the following classification problem: given a set of expertly labeled side data containing C different classes (e.g., variable star types), where measurements can be made on the classes in question to extract a set of feature spaces for each observation, how do we define a distance metric that optimizes the misclassification rate? Specifically, how can this be done within the context of variable star classification based on the observation of photometric time-domain data? We have identified a number of features that provide utility in discriminating between various types of stellar variables. We review how to combine this information together and generate a decision space; or rather, how to define the distance $d_{ij} = (x_i - x_j)' \mathbf{M} (x_i - x_j)$, when x_i contains two matrices (SSMM or DF in our case). Specifically we attempt to construct a distance metric based on multiple attributes of different dimensions (e.g. $\mathbb{R}^{m \times n}$ and $\mathbb{R}^{m \times 1}$).

To respond to this challenge we investigate the utility of multi-view learning. For our purposes here we specify each individual measurement as the feature, and the individual transformations or representations of the underlying measurement as the feature space. Views, are the generic independent collections of these features or feature space. Thus, if provided the color of a variable star in *ugriz*, the individual measurements of $u - g$ or $r - i$ shall be referred to here as the features but the collective set of colors is the feature space. Our methodology here allows us to defined sets of collections of these feature and/or feature spaces as independent views, for example: all of *ugriz* measurements, the vectorized DF measurement, the concatenation of time-domain statistics and colors, the reduced (selected) sampling of Fourier spectra, could all be individual views. The expert defined these views *a priori*.

Xu et al. (2013) and Kan et al. (2016) review multi-view learning and outline some basic definitions. Multi-view learning treats the individual views separately, but also provides some functionality for joint learning where the importance of each view is dependent on the others. As an alternative to multi-view learning, the multiple views could be transformed into a single view, usually via concatenation. The cost-benefit analysis of concatenated single-view vs. multi-view learning are discussed in Xu et al. (2013) and are beyond the scope of this paper.

Classifier fusion (Kittler et al. 1998; Tax 2001; Tax and Muller 2003) could be considered as an alternative to multi-view learning, with each view independently learned, and resulting in an independent classification algorithm. The result of the set of these classifiers are combined together (mixing of posterior probability) to result in a singular estimate of classification/label; this is similar to the operation of a Random Forest classifier, i.e. results from multiple individual trees combined together to form a joint estimate. We differentiate between the single-view learning with concatenation, multi-view learning, and classifier fusion

designs based on when the join of the views is considered in the optimization process: before, during, or after.

Multi-view learning can be divided into three topics: 1) co-training, 2) multiple-kernel learning, and 3) subspace learning. Each method attempts to consider all views during the training process. Multiple-kernel learning algorithms attempt to exploit kernels that naturally correspond to different views and combine kernels either linearly or non-linearly to improve learning performance (Gönen and Alpaydın 2011; Kan et al. 2016).

Sub-space learning uses canonical correlation analysis (CCA), or a similar method, to generate an optimal latent representation of two views which can be trained on directly. The CCA method can be iterated multiple times based on the number of views, this process will frequently result in a dimensionality that is lower than the original space (Hotelling 1936; Akaho 2006; Zhu et al. 2012; Kan et al. 2016).

This work will focus on a method of co-training, specifically metric co-training. Large Margin Multi-Metric Learning (Hu et al. 2014, 2018) is an example of metric co-training; the designed objective function minimizes the optimization of the individual view, as well as the difference between view distances, simultaneously. The full derivation of this algorithm is outlined in Hu et al. (2014), and the algorithm for optimization for LM³L is given as their Algorithm 1. We have implemented the algorithm in Java and it is available as part of the software distribution.

Our implementation also includes additional considerations not discussed in the original reference. These considerations were found to be necessary based on challenges discovered when we applied the LM³L algorithm to our data. The challenges and our responses are discussed in Appendix A.

In addition to the implementation of LM³L, we have developed a matrix variate version as well (section 2.4). This matrix variate classifier is novel with respect to multi-view learning methods and is one of two metric learning methods that we know of, the other being Push-Pull Metric Learning (Helfer et al. 2015).

2.4. Large Margin Multi-View Metric Learning with Matrix Variates

The literature on metric learning methods is fairly extensive (see Bellet et al. (2015) for a review), however all of the methods presented so far focus on the original definition that is based in $X \subseteq \mathbb{R}^{d \times 1}$, i.e. vector-variate learning. While the handling of matrix-variate data has been addressed here, the method requires a transformation— $\text{vec}(x)$ and then ECVA—which ignores the problem of directly operating on matrix-variate data. The literature on matrix-variate classification and operations is fairly sparse. The idea of a metric learning supervised classification methodology based on matrix-variate data is novel.

Most of the matrix-variate research has some roots in the work by Hotelling (1936) and Dawid (1981). There are some key modern references to be noted as well: Ding and Cook (2014) and Ding and Dennis Cook (2018) address matrix-variate PCA and matrix variate regression (matrix predictor and response), Dutilleul (1999) and Zhou et al. (2014) address the mathematics of the matrix normal distribution, and Safayani and Shalmani (2011) address matrix-variate CCA.

Developing a matrix-variate metric learning algorithm requires a formal definition of distance for matrix-variate observations, i.e. where $X \subseteq \mathbb{R}^{p \times q}$. Glanz and Carvalho (2013) define the matrix normal distribution as $X_i \sim MN(\mu, \Sigma_s, \Sigma_c)$, where X_i and μ are $p \times q$ matrices, Σ_s is a $p \times p$ matrix defining the row

covariance, and Σ_c is a $q \times q$ matrix defining the column covariance. Equivalently the relationship between the matrix normal distribution and the vector normal distribution is given as equation 5,

$$\text{vec}(X_i) \sim N(\text{vec}(\mu), \Sigma_c \otimes \Sigma_s). \quad (5)$$

The matrix-variate normal distribution is defined as equation 6 (Gupta and Nagar 2000)

$$P(X_i; \mu, \Sigma_s, \Sigma_c) = (2\pi)^{-\frac{pq}{2}} |(\Sigma_c \otimes \Sigma_s)^{-1}|^{\frac{1}{2}} \exp \left\{ -\frac{1}{2} \text{vec}(X_i - \mu)^T (\Sigma_c \otimes \Sigma_s)^{-1} \text{vec}(X_i - \mu) \right\}. \quad (6)$$

This distribution holds for the features that we are using as part of this study, at least within the individual classes. The Mahalanobis distance between our observations is then defined for the Matrix-Variate case as equations 7 to 9:

$$d_{\Sigma}(X, X') \doteq \text{vec}(X - X')^T (\Sigma_c \otimes \Sigma_s)^{-1} \text{vec}(X - X'), \quad (7)$$

$$= \text{vec}(X - X')^T \text{vec}(\Sigma_s^{-1} (X - X') \Sigma_c^{-1}), \quad (8)$$

$$= \text{tr}[\Sigma_c^{-1} (X - X')^T \Sigma_s^{-1} (X - X')]. \quad (9)$$

This last iteration of the distance between matrices is used in our development of a metric learning methodology. Similar to the development of LM³L and the outline of Torresani and Lee (2007), we develop a metric learning algorithm for matrix-variate data. First the Mahalanobis distance for the matrix-variate multi-view case is recast as equation 10

$$d_{\mathbf{U}_k, \mathbf{V}_k}(X_i^k, X_j^k) = \text{tr}[\mathbf{U}_k (X_i^k - X_j^k)^T \mathbf{V}_k (X_i^k - X_j^k)]; \quad (10)$$

where \mathbf{U}_k and \mathbf{V}_k represent the inverse covariance of the column and row respectively. The individual view objective function is constructed similar to the LMNN (Weinberger et al. 2009) methodology; we define a push (equation 11) and pull (equation 12) as:

$$\begin{aligned} \text{push}_k = \gamma \sum_{j \rightsquigarrow i, l} \eta_{ij}^k (1 - y_{il}) \\ \cdot h[d_{\mathbf{U}_k, \mathbf{V}_k}(X_i^k, X_j^k) - d_{\mathbf{U}_k, \mathbf{V}_k}(X_i^k, X_l^k) + 1], \end{aligned} \quad (11)$$

$$\text{pull}_k = \sum_{i, j} \eta_{ij}^k \cdot d_{\mathbf{U}_k, \mathbf{V}_k}(X_i^k, X_j^k); \quad (12)$$

where $y_{il} = 1$ if and only if $y_i = y_l$ and $y_{il} = 0$ otherwise; and $\eta_{ij}^k = 1$ if and only if x_i and x_j are targeted neighbors of similar label $y_i = y_j$. For a more in-depth discussion of target neighbor, see Torresani and Lee (2007).

Furthermore, we include regularization terms (Schultz and Joachims 2004) with respect to \mathbf{U}_k and \mathbf{V}_k as part of the objective function design; these are defined as $\lambda \|\mathbf{U}_k\|_F^2$ and $\lambda \|\mathbf{V}_k\|_F^2$,

respectively. The inclusion of regularization terms in our objective function help promote sparsity in the learned metrics. Favoring sparsity can be beneficial when the dimensionality of the feature spaces is high, and can help lead to a more generic and stable solution.

The sub-view objective function is then equation 13:

$$\min_{\mathbf{U}_k, \mathbf{V}_k} I_k = \sum_{i,j} \eta_{ij}^k \cdot d_{\mathbf{U}_k, \mathbf{V}_k}(X_i^k, X_j^k) + \gamma \sum_{j \sim i, l} \eta_{ij}^k (1 - y_{il}) \cdot h \left[d_{\mathbf{U}_k, \mathbf{V}_k}(X_i^k, X_j^k) - d_{\mathbf{U}_k, \mathbf{V}_k}(X_i^k, X_l^k) + 1 \right] + \lambda \|\mathbf{U}_k\|_F^2 + \lambda \|\mathbf{V}_k\|_F^2; \quad (13)$$

where $\lambda > 0$ and controls the importance of the regularization. From LM³L the objective function is equation 14:

$$\min_{\mathbf{U}_k, \mathbf{V}_k} J_k = w_k I_k + \mu \sum_{q=1, q \neq k}^K \sum_{i,j} \left(d_{\mathbf{U}_k, \mathbf{V}_k}(X_i^k, X_j^k) - d_{\mathbf{U}_q, \mathbf{V}_q}(X_i^q, X_j^q) \right)^2; \quad (14)$$

where $\sum_{k=1}^K w_k = 1$ and the first term is the contribution of the individual k^{th} view, while the second term is designed to minimize the distance difference between attributes. Using these objective function definitions, we derive the gradient descent optimization procedure in Appendix B following a similar procedures used by Weinberger et al. (2009). The resulting methodology is proposed in Algorithm 1.

Algorithm 1 LM³L-MV Algorithm Flow

Require: $\rho \geq 1$

Ensure: X_k

```

1: while  $|J^{(t)} - J^{(t-1)}| < \epsilon$  do
2:   for  $k = 1, \dots, K$  do
3:     Solve  $\nabla J_k(X_i^k, U_k, V_k) = \left[ \frac{\partial J_k}{\partial \Gamma_k}, \frac{\partial J_k}{\partial \mathbf{N}_k} \right]$ 
4:      $\hat{\beta}_k^t = \frac{1}{2} \cdot \frac{Tr[\Delta g(\Gamma_k) \cdot \Delta \Gamma_k^H + \Delta \Gamma_k \cdot \Delta g(\Gamma_k)^H]}{Tr[\Delta g(\Gamma_k) \cdot \Delta g(\Gamma_k)^H]}$ 
5:      $\hat{\kappa}_k^t = \frac{1}{2} \cdot \frac{Tr[\Delta g(\mathbf{N}_k) \cdot \Delta \mathbf{N}_k^H + \Delta \mathbf{N}_k \cdot \Delta g(\mathbf{N}_k)^H]}{Tr[\Delta g(\mathbf{N}_k) \cdot \Delta g(\mathbf{N}_k)^H]}$ 
6:      $\Gamma_k^{(t+1)} = \Gamma_k^{(t)} - \beta_k^{(t)} \frac{\partial J_k}{\partial \Gamma_k}$ 
7:      $\mathbf{N}_k^{(t+1)} = \mathbf{N}_k^{(t)} - \kappa_k^{(t)} \frac{\partial J_k}{\partial \mathbf{N}_k}$ 
8:   end for
9:   for  $k = 1, \dots, K$  do
10:     $w_k = \frac{(1/I_k)^{1/(p-1)}}{\sum_{k=1}^K (1/I_k)^{1/(p-1)}}$ 
11:     $J_k = w_k I_k$ 
12:     $+= \mu \sum_{q=1, q \neq k}^K \sum_{i,j} \left( d_{\mathbf{U}_k, \mathbf{V}_k}(X_i^k, X_j^k) - d_{\mathbf{U}_q, \mathbf{V}_q}(X_i^q, X_j^q) \right)^2$ 
13:     $J^{(t)} = J^{(t)} + J_k$ 
14:   end for
15: end while
return  $\mathbf{U}_k = \Gamma_k^T \Gamma_k$  and  $\mathbf{V}_k = \mathbf{N}_k^T \mathbf{N}_k$ 

```

3. Implementation

We develop a supporting functional library in Java (java-jdk/11.0.1), and rely on a number of additional publicly available scientific and mathematical open source packages including the Apache foundation commons packages (e.g. Math Commons

Foundation 2018b and Commons Lang Foundation 2018c) and the JSOFA package to support our designs. The overall functionality is supported at a high level by the following open source packages:

- Maven is used to manage dependencies, and produce executable functionality from the project Foundation (2018a)
- JUnit is used to support library unit test management (Team 2018a)
- slf4j is used as a logging frame work (Team 2017)
- MatFileRW is used for I/O handling (Team 2018b)

We recommend reviewing the vsa-parent .pom file included as part of the software package for a more comprehensive review of the functional dependency. Versions are subject to upgrades as development proceeds beyond this publication. Python developer should note that the library outlined here can be easily accessed using any number of Python-to-Java projects (Py4J and Jython for example).

Execution of the code was performed on a number of platforms including a personal laptop (MacBook Pro, 2.5GHz Intel Core i7, macOS Mojave) and an institution high performance computer (Florida Institute of Technology, BlueShark HPC)³. The development of the library and functionality in Java allow for the functionality presented here to be applied regardless of platform.

We are not reporting processing times as part of this analysis as the computational times varied depending on platform used. Our initial research included using the parallel computing functionality packaged with Java, in combination with the GPU functionality on the BlueShark computer. Further research is necessary to quantify optimal implementation with respect to convergence speed and memory usage.

3.1. Training Data

Similar to Johnston and Peter (2017), we use the University of California Riverside Time Series Classification Archive (UCR) and the Lincoln Near-Earth Asteroid Research (LINEAR) dataset to demonstrate the performance of our feature space classifier. The individual datasets are described as follows:

- **UCR:** We baseline the investigated classification methodologies (Keogh et al. 2011) using the UCR time domain datasets. The UCR time domain dataset STARLIGHT (Protopapas et al. 2006) is derived from a set of Cepheid, RR Lyra, and Eclipsing Binary Stars. This time-domain dataset is phased (folded) via the primary period and smoothed using the SUPER-SMOOTHER algorithm (Reimann 1994) by the Protopapas study prior to being provided to the UCR database. Note that the sub-groups of each of the three classes are combined together in the UCR data (i.e., RR Lyr (ab) + RR Lyr (c) = RR).
- **LINEAR:** The original database LINEAR is subsampled; we select time series data that has been verified and for which accurate photometric values are available (Sesar et al. 2011; Palaversa et al. 2013). This subsampled set is parsed into separate training and test sets. From the starting sample of 7,194 LINEAR variables, a clean sample of 6,146 time series datasets and their associated photometric values is used. Stellar class-type is limited further to the top five most populous classes: RR Lyr (ab), RR Lyr (c), Delta Scuti / SX Phe,

³ <https://it.fit.edu/information-and-policies/computing/blueshark-supercomputer-hpc/>

Contact Binaries and Algol-Like Stars with 2 Minima, resulting in a set of 6,086 time series datasets.

Training data subsets are generated as follows: UCR already defines a training and test set, the LINEAR data is split into a training and test set using a predefined algorithm (random assignment, of nearly equal representation of classes in training and test). We used a method of 5-fold cross-validation both datasets; the partitions in 5-fold algorithm are populated via random assignment. For more details on the datasets themselves, a baseline for performance, and additional references, see Johnston and Peter (2017).

3.2. Feature Optimization

The time domain transformation we selected requires parameter optimization (resolution, kernel size, etc.); each survey can potentially have a slightly different optimal set of transformation parameters with respect to the underlying survey parameters (e.g. sample rate, survey frequency, number of breaks over all observations, etc.). While we could include the parameters optimization in the cross-validation process for the classifier, this will be highly computationally challenging, specifically for classifier that require iterations, as we would be handling an increasing number of permutations with each iteration, over an unknown number of iteration. To address this problem, the feature space is cross-validated on the training dataset, and k-NN classification is used (assuming a fixed temporary k value allows little to no tuning) to estimate the misclassification error with the proposed feature space parameters. The optimized features are used as givens for the cross-validation process in optimizing the intended classifier. Likely some loss of performance will occur, but considering how the final classifier design is based on k-NN as well, it is expected to be minor.

Because of the multi-dimensional nature of our feature space, we propose the following method for feature optimization—per class we generate a mean representation of the feature (given the fraction of data being trained on), all data are then transformed (training and cross-validation data) via Park et al. (2003) into a distance representation, i.e. the difference of the observed feature and each of the means is generated. Note that for the matrix feature spaces, the Frobenius Norm is used. Alternatively we could have generated means based on unsupervised clustering (k-Means); while not used in this study, this functionality is provided as part of the code. We found that the performance using the unsupervised case was very sensitive to the initial number of k used. For the LINEAR and UCR datasets, the results were found with respect to optimization of feature (DF and SSMM) parameters to be roughly the same. A k-NN algorithm is applied to the reduced feature space, 5-fold classification is then used to generate the estimate of error, and the misclassification results are presented a response map given feature parameters (Figures 3 and Figure 4):

We select the optimum values for each feature space, based on a minimization of both the LINEAR and UCR data. These values are estimated to be: DF Optimized (x, y) – 30×25, SSMM Optimized (res x scale) – 0.06 × 35.0

3.3. Large Margin Multi-view Metric Learning Implementation

The implementation of LM³L is applied to the UCR and LINEAR datasets. Based on the number of views associated with each feature set, the underlying classifier will be different (e.g. UCR does not contain color information and it also has only

Table 1. The cross-validation process for LM³L tunable values for each of the seven experimental settings. τ and η define the large margin threshold, μ controls the importance of pairwise distance between views

Variable	1	2	3	4	5	6	7
τ	1	1.75	0.25	1	1	1	1
η	5	5	5	8	2	5	5
μ	0.5	0.5	0.5	0.5	0.5	1.0	0.1

three classes compared to LINEAR’s five). The features SSMM, DF, and Statistical Representations (mean, standard deviation, kurtosis, etc.) are computed for both datasets. Color and the time domain representations provided with the LINEAR data are also included as additional views.

To allow for the implementation of the vector-variate classifier, the dimensionality of the SSMM and DF features are reduced via vectorization of the matrix and then processing by the ECVA algorithm, resulting in a dimensionality that is $k-1$, where k is the number of classes. We note that without this processing via ECVA, the times for the optimization became prohibitively long, this is similar to the implementation of IPMML given in Zhou et al. (2016). SSMM and DF features are generated with respect to the LINEAR dataset—Park’s transformation is not applied here—the feature space reduced via ECVA, the results are and given in Figure 5 (DF) and Figure 6 (SSMM).

Similarly, the SSMM and DF features are generated for the UCR dataset—Park’s transformation is not applied here—and the feature space reduced via ECVA. The results are plotted and given in Figure 7 (DF–Left) and (SSMM–Right).

The dimensions given in the figures are reduced dimensions resulting from the ECVA transform and therefore they do not necessarily have meaningful descriptions (besides $x_1, x_2, x_3, \dots, x_n$). These reduced feature spaces are used as input to the LM³L algorithm.

The individual views are standardized (subtract by mean and divide by standard deviation). Cross-validation of LM³L is used to optimize the three tunable parameters and the one parameter associated with the k-NN. The LM³L authors recommend some basic parameter starting points; our analysis includes investigating the tunable values as well as an upper (+1) and lower (-1) level about each parameter, over a set of odd k-NN values [1,19]; the optimization only needs to occur for each set of tunable values, the misclassification given a k-Value can be evaluated separately, this experiment is outlined in Table 1.

Cross-validation is performed to both optimize for our application and investigate the sensitivity of the classifier to adjustment of these parameters. For a break down of the cross validation results, see the associated datasets and spreadsheet provided as part of the digital supplement.

3.3.1. Testing and Results (UCR & LINEAR)

Based on the cross-validation process, the following optimal parameters are found:

- LINEAR: k-NN(11), τ (1.0), η (5.0), μ (0.1)
- UCR: k-NN(9), τ (1.0), η (5.0), μ (0.1)

The classifier is then trained using the total set of training data along with the optimal parameters selected. Given Hu et al. (2014) definitions: μ controls the importance of pairwise distance between views in the optimization process, τ and η define

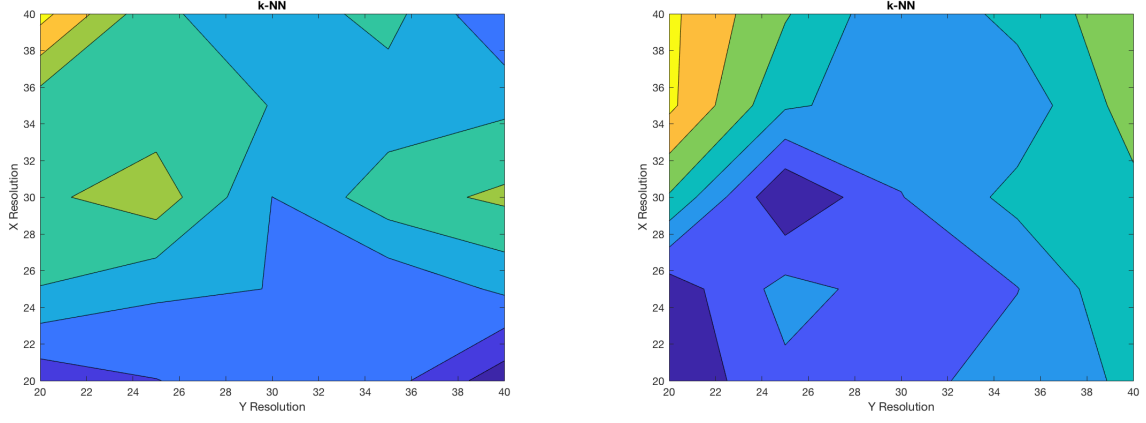


Fig. 3. Parameter optimization of the Distribution Field feature space (Left: UCR Data, Right: LINEAR Data)

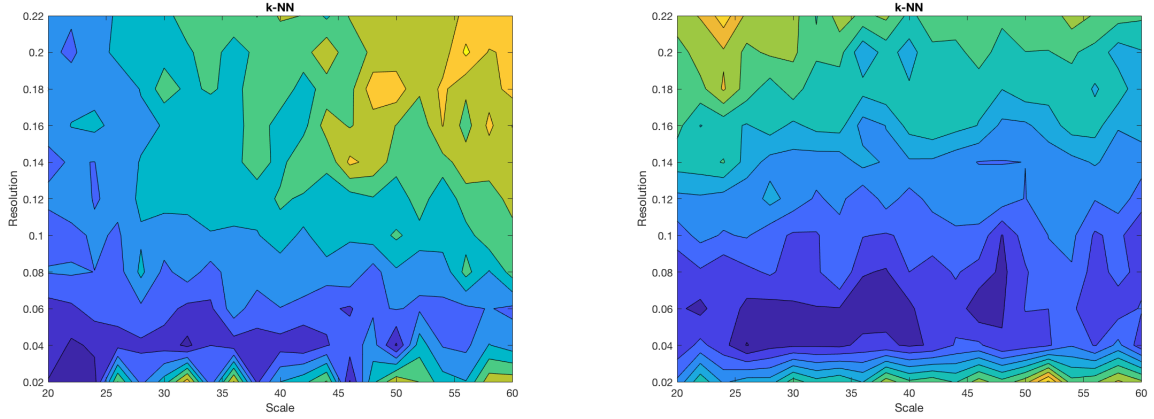


Fig. 4. Parameter optimization of the SSMM feature space (Left: UCR Data, Right: LINEAR Data)

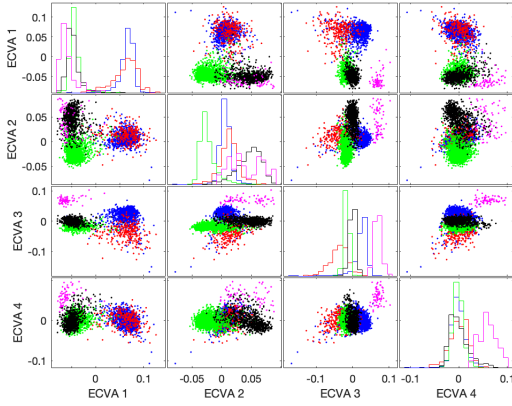


Fig. 5. DF Feature space after ECVA reduction from LINEAR (Contact Binary/blue circle, Algol/ red +, RR (ab)/green points, RR (c) in black squares, Delta Scu/SX Phe magneta diamonds) off-diagonal plots represent comparison between two different features, on-diagonal plots represent distribution of classes within a feature (one dimensional)

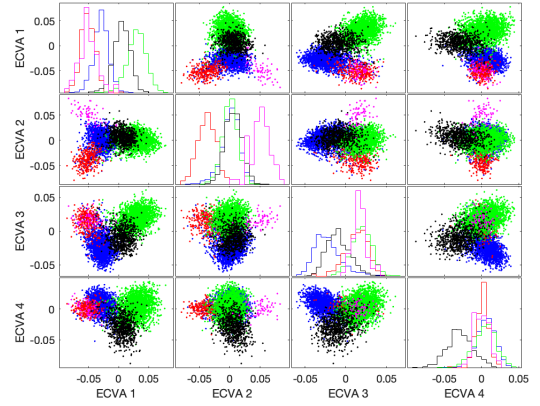


Fig. 6. SSMM feature space after ECVA reduction LINEAR (Contact Binary/blue circle, Algol/ red +, RR (ab)/green points, RR (c) in black squares, Delta Scu/SX Phe magneta diamonds) off-diagonal plots represent comparison between two different features, on-diagonal plots represent distribution of classes within a feature (one dimensional). The dimension plotted are the first 4 canonical variates (transformed DF space).

the threshold $y_{ij}(\eta_k - d_{M_k}^2(x_i^k, x_j^k)) > \tau_k$ used as the margin definition. The trained classifier is applied to the test data, the confusion matrices (Fawcett 2006) resulting from the application are presented in Table 2 and Table 3:

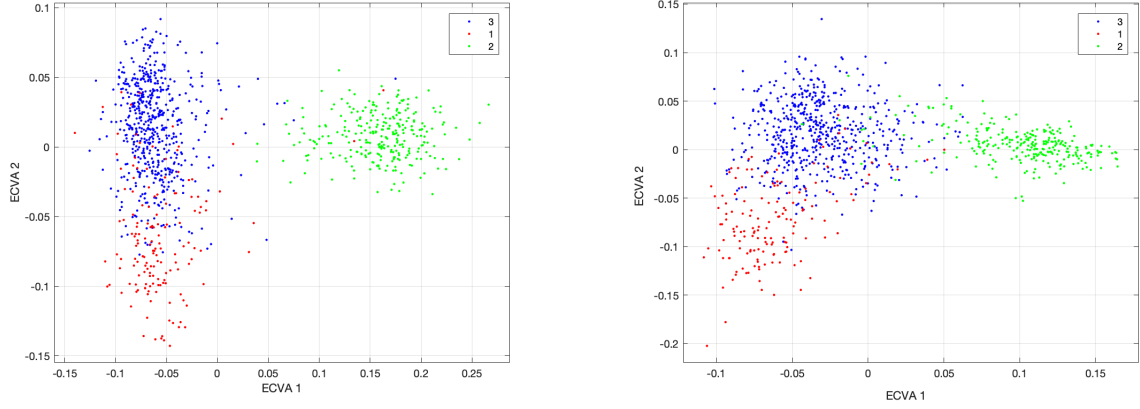


Fig. 7. DF–Left and SSMM–Right feature space after ECVA reduction from UCR. Class names (1,2, and 3) are based on the classes provided by the originating source and the UCR database. The dimension plotted are the first 2 canonical variates (transformed DF space).

Table 2. LINEAR confusion matrix via LM³L entries are counts (percent)

Misclassification Rate	RR Lyr (ab)	Delta Scu / SX Phe	Algol	RR Lyr (c)	Contact Binary	Missed
RR Lyr (ab)	1081 (0.992)	0 (0.000)	0 (0.000)	6 (0.006)	1 (0.001)	2 (0.002)
Delta Scu / SX Phe	0 (0.000)	23 (0.852)	0 (0.000)	2 (0.074)	2 (0.074)	0 (0.000)
Algol	1 (0.007)	0 (0.000)	108 (0.788)	0 (0.000)	28 (0.204)	0 (0.000)
RR Lyr (c)	23 (0.062)	0 (0.000)	1 (0.003)	343 (0.925)	4 (0.011)	0 (0.000)
Contact Binary	3 (0.003)	0 (0.000)	29 (0.033)	9 (0.010)	832 (0.952)	1 (0.001)

Table 3. UCR confusion matrix via LM³L entries are counts (percent)

Misclassification Rate	2	3	1	Missed
2	2296 (0.996)	9 (0.004)	0 (0.000)	0 (0.000)
3	17 (0.004)	4621 (0.972)	116 (0.023)	0 (0.000)
1	8 (0.007)	375 (0.319)	794 (0.675)	0 (0.000)

3.4. Large Margin Multi-View Metric Learning with Matrix Variates Implementation

The implementation of LM³L-MV is applied to the UCR and LINEAR datasets. The features SSMM, DF, and Statistical Representations (mean, standard deviation, kurtosis, etc.) are computed for both datasets. Similar to the LM³L procedure, color and the time domain representations provided with the LINEAR data are also included as additional views. The implementation of the matrix-variate classifier, allows us to avoid the vectorization and feature reduction (ECVA) step. The individual views are standardized prior to optimization. Also similar to the LM³L procedure, cross-validation of LM³L-MV is used to optimize the three tunable parameters and the one parameter associated with the k-NN. The table of explored tunable parameters is given in Table 4:

For a break down of the results, see the associated datasets and spreadsheet provided as part of the digital supplement.

3.4.1. Testing and Results (UCR & LINEAR)

Based on the cross-validation process, the following optimal parameters are found (and their cross-validation error estimates):

- *LINEAR*: k-NN(15), $\lambda(0.5)$, $\mu(0.5)$, $\gamma(0.5)$
- *UCR*: k-NN(19), $\lambda(0.5)$, $\mu(1.0)$, $\gamma(0.5)$

The classifier is then trained using the total set of training data along with the optimal parameters selected. The λ parameter

controls the importance of regularization, the μ parameter controls the importance of pairwise distance in the optimization process, and γ controls the balance between push and pull.

The trained classifier is applied to the test data, the confusion matrices resulting from the application are presented in Table 5 and Table 6:

3.5. Comparison

The matrix-variate and the vector-variate versions do not perform much different under the conditions provided given the data observed. However, as a reminder, the LM³L implementation includes a feature reduction methodology (ECVA) that our LM³L-MV does not. The ECVA front end was necessary as the dimensionality of the unreduced input vectors results in features and metrics which are prohibitively large (computationally). It is not entirely surprising that our two competitive methodologies perform similarly (see Tables C.1 and C.2), with the LM³L algorithm of having the benefit of being able to process the matrix-variate spaces ahead of time via ECVA and thus being able to process the SSMM and DF features spaces in a lower dimension ($c - 1$ dimensions). For a quantitative comparison of our classifiers, we have computed precision and recall metrics for our presented classifiers (Fawcett 2006; Sokolova and Lapalme 2009) as well as an overall estimate of F1-score, the results of this analysis are presented in Table 7. However, a direct one-to-one comparison to other pattern classification methods is diffi-

Table 4. The cross-validation process for LM³L-MV tunable values

Variable	1	2	3	4	5	6	7
λ	0.5	1.0	0.25	0.5	0.5	0.5	0.5
μ	0.5	0.5	0.5	1.0	0.25	0.5	0.5
γ	0.5	0.5	0.5	0.5	0.5	1.0	0.25

Table 5. LINEAR confusion matrix via LM³L-MV entries are counts (percent)

Misclassification Rate	RR Lyr (ab)	Delta Scu / SX Phe	Algol	RR Lyr (c)	Contact Binary	Missed
RR Lyr (ab)	1074 (0.985)	0 (0.000)	1 (0.001)	15 (0.014)	0 (0.000)	0 (0.000)
Delta Scu / SX Phe	1 (0.037)	24 (0.889)	0 (0.000)	2 (0.074)	0 (0.000)	0 (0.000)
Algol	3 (0.022)	0 (0.000)	104 (0.759)	1 (0.007)	29 (0.212)	0 (0.000)
RR Lyr (c)	23 (0.059)	0 (0.000)	1 (0.003)	343 (0.930)	4 (0.008)	0 (0.000)
Contact Binary	3 (0.003)	0 (0.000)	29 (0.035)	9 (0.001)	832 (0.958)	1 (0.002)

Table 6. UCR confusion matrix via LM³L-MV entries are counts (percent)

Misclassification Rate	2	3	1	Missed
2	2298 (0.997)	6 (0.003)	0 (0.000)	1 (~0.000)
3	4 (0.001)	4450 (0.936)	300 (0.063)	0 (0.000)
1	3 (0.003)	467 (0.397)	707 (0.601)	0 (0.000)

cult, as there are no other classifiers that we know of that are both multi-view and matrix-variate.

We can still provide some context by looking at known alternatives that may partially address our particular situation. We have included results based on the implementation of a multi-view k-NN classifier (B.10) in both the matrix-variate and vector-variate domains, but with the metrics being the identity matrix (i.e. Euclidean and Forbinus distances respectively), as a baseline reference point. Similarly, we have included results based on the implementation of a single view k-NN classifier (B.10) applied to the vectorized and concatenated features (i.e. Euclidean distance).

For comparison we include classifiers generated from the main individual feature spaces; optimization was performed using Random Forest classification (Breiman et al. 1984). In addition to these standard methods applied to the unreduced feature space/views, we have generated classifiers based on the dimensionally reduced feature space generated resulting from the ECVA algorithm applied to the DF and SSMM vectorized feature spaces. These reduced feature spaces/views are implemented using the Zhou et al. (2016) IPMML (i.e., multi-view algorithm), this implementation is the nearest similar implementation to both our LM³L and LM³L-MV algorithm designs. Detailed computations associated with all analyses are included as part of the digital supplement.

It should be noted, that ECVA has its limitations; anecdotally on more than one occasion during the initial analysis, when the full dataset was provided to the algorithm, the memory of the machine was exceeded. Care was taken with the LINEAR dataset to develop a training dataset that was small enough that the out-of-memory error would not occur, but a large enough that each of the class-types was represented sufficiently. Similarly, the projection into lower dimensional space meant that the LM³L implementation iterated at a much faster rate with the same amount of data, compared to the LM³L-MV algorithm. The matrix multiplication operations associated with the matrix distance computation are more computationally expensive compared to the simpler vector metric distance computation, however many computational languages have been optimized for ma-

Table 7. F1-Score metrics for the proposed classifiers with respect to LINEAR and UCR datasets

F1-Score	UCR	LINEAR
LM ³ L	0.904	0.918
LM ³ L-MV	0.860	0.916
IPMML	0.900	0.916
k-NN Multi-View MV	0.725	0.574
k-NN Multi-View	0.691	0.506
k-NN Concatenated	0.650	0.427
RF – DF	0.878	0.650
RF – SSMM	0.659	0.402
RF – Time Statistics	0.678	0.787

trix multiplication (e.g., MATLAB, Mathematica, CUDA, etc.). Again, the time the ECVA algorithm takes to operate upfront saves the LM³L iterations time. In general, both algorithms perform well with respect to misclassification rate, but both also require concessions to handle the scale and scope of the feature spaces used. The cost of most of these concession can be mitigated with additional machine learning strategies, some of which we have begun to implement here—parallel computation for example.

4. Conclusions

The classification of variable stars relies on a proper selection of features of interest and a classification framework that can support the linear separation of those features. Features should be selected that quantify the signature of the variability, i.e. its structure and information content. Here, two features which have utility in providing discriminatory capabilities, the SSMM and DF feature spaces are studied. The feature extraction methodologies are applied to the LINEAR and UCR dataset, as well as a standard breakdown of time domain descriptive statistics, and in the case of the LINEAR dataset, a combination of *ugriz* colors. To support the set of high-dimensionality features, or views, multi-view metric learning is investigated as a viable design.

Multi-view learning provides an avenue for integrating multiple transforms to generate a superior classifier. The structure of multi-view metric learning allows for a number of modern computational designs to be used to support increasing scale and scope (e.g., parallel computation); these considerations can be leveraged given the parameters of the experiment designed or the project in question.

Presented, in addition to an implementation of a standard multi-view metric learning algorithm (LM³L) that works with a feature space that has been vectorized and reduced in dimension, is a multi-view metric learning algorithm designed to work with matrix-variate views. This new classifier design does not require transformation of the matrix-variate views ahead of time, and instead operates directly on the matrix data. The development of both algorithm designs (matrix-variate and vector-variate) with respect to the targeted experiment of interest (discrimination of time-domain variable stars) highlighted a number of challenges to be addressed prior to practical application. In overcoming these challenges, it was found that the novel classifier design (LM³L-MV) performed on order of the staged (Vectorization + ECVA + LM³L) classifier. Future research will include investigating overcoming high dimensionality matrix data (e.g. SSMM), improving the parallelization of the design presented, and implementing community standard workarounds for large dataset data (i.e., on-line learning, stochastic/batch gradient descent methods, k-d tree... etc.).

Acknowledgements

The authors are grateful for the valuable machine learning discussion with S. Wiechecki Vergara. Inspiration provided by C. Role. Research was partially supported by Perspecta, Inc. This material is based upon work supported by the NASA Florida Space Grant under 2018 Dissertation And Thesis Improvement Fellowship (No. 202379). The LINEAR program is sponsored by the National Aeronautics and Space Administration (NRA Nos. NNH09ZDA001N, 09-NEOO09-0010) and the United States Air Force under Air Force Contract FA8721-05-C-0002. This material is based upon work supported by the National Science Foundation under Grant No. CNS 09-23050.

References

- S. Akaho. A kernel method for canonical correlation analysis. *arXiv preprint cs/0609071*, 2006.
- N. S. Altman. An introduction to kernel and nearest-neighbor nonparametric regression. *The American Statistician*, 46(3):175–185, 1992.
- R. Angeloni, R. Contreras Ramos, M. Catelan, et al. The VVV Templates Project Towards an automated classification of VVV light-curves. I. Building a database of stellar variability in the near-infrared. *A&A*, 567:A100, July 2014.
- D. J. Armstrong, J. Kirk, K. W. F. Lam, et al. K2 variable catalogue - II. Machine learning classification of variable stars and eclipsing binaries in K2 fields 0-4. *MNRAS*, 456:2260–2272, February 2016.
- J. Barzilai and J. M. Borwein. Two-point step size gradient methods. *IMA journal of numerical analysis*, 8(1):141–148, 1988.
- G. Bass and K. Borne. Supervised ensemble classification of Kepler variable stars. *MNRAS*, 459:3721–3737, July 2016.
- A. Bellet, A. Habrard, and M. Sebban. Metric learning. *Synthesis Lectures on Artificial Intelligence and Machine Learning*, 9(1):1–151, 2015.
- J. Blomme, L. M. Sarro, F. T. O'Donovan, et al. Improved methodology for the automated classification of periodic variable stars. *MNRAS*, 418:96–106, November 2011.
- V. J. Bolós and R. Benítez. The Wavelet Scalogram in the Study of Time Series. In *Advances in Differential Equations and Applications*, volume 4, pages 147–154. SEMA SIMAI Springer Series, 10 2014.
- R. Bos, S. de Waele, and P. M. T. Broersen. Autoregressive spectral estimation by application of the Burg algorithm to irregularly sampled data. *Instrumentation and Measurement, IEEE Transactions on*, 51(6):1289–1294, Dec 2002.
- L. Breiman, J. Friedman, C. J. Stone, and R. A. Olshen. *Classification and regression trees*. CRC press, 1984.
- P. M. Broersen. Practical aspects of the spectral analysis of irregularly sampled data with time-series models. *IEEE Transactions on Instrumentation and Measurement*, 58(5):1380–1388, 2009.
- V. Chandola, A. Banerjee, and V. Kumar. Anomaly detection: A survey. *ACM Computing Surveys (CSUR)*, 41(3):15, 2009.
- A. P. Dawid. Some matrix-variate distribution theory: notational considerations and a Bayesian application. *Biometrika*, 68(1):265–274, 1981.
- J. Debusscher. *Automated Classification of variable stars: Application to the OGLE and CoRoT databases*. PhD thesis, Institute of Astronomy, Katholieke Universiteit Leuven, Belgium, 2009.
- S. Ding and R. D. Cook. Dimension folding PCA and PFC for matrix-valued predictors. *Statistica Sinica*, 24(1):463–492, 2014.
- S. Ding and R. Dennis Cook. Matrix variate regressions and envelope models. *Journal of the Royal Statistical Society: Series B (Statistical Methodology)*, 80(2):387–408, 2018.
- A. D'Isanto, S. Cavuoti, M. Brescia, et al. An analysis of feature relevance in the classification of astronomical transients with machine learning methods. *MNRAS*, 457:3119–3132, April 2016.
- R. O. Duda, P. E. Hart, and D. G. Stork. *Pattern classification*. John Wiley & Sons, 2012.
- P. Dutilleul. The MLE algorithm for the matrix normal distribution. *Journal of statistical computation and simulation*, 64(2):105–123, 1999.
- C. Faloutsos, M. Ranganathan, and Y. Manolopoulos. *Fast subsequence matching in time-series databases*, volume 23. ACM, 1994.
- T. Fawcett. An introduction to ROC analysis. *Pattern recognition letters*, 27(8): 861–874, June 2006.
- Apache Software Foundation. Apache maven. Apache Software Foundation, 2018a. URL <https://maven.apache.org/index.html>.
- Apache Software Foundation. Apache math commons. Apache Software Foundation, 2018b. URL <http://commons.apache.org/proper/commons-math/>.
- Apache Software Foundation. Apache commons lang. Apache Software Foundation, 2018c. URL <https://commons.apache.org/proper/commons-lang/>.
- J.H. Friedman. A variable span smoother. Technical report, Stanford Univ CA lab for computational statistics, 1984.
- B. D. Fulcher, M. A. Little, and N. S. Jones. Highly comparative time-series analysis: the empirical structure of time series and their methods. *Journal of the Royal Society Interface*, 10(83):20130048, 2013.
- P. A. Gagniac. *Markov Chains: From Theory to Implementation and Experimentation*. John Wiley & Sons, 2017.
- X. Ge and P. Smyth. Deformable Markov model templates for time-series pattern matching. In *Proceedings of the sixth ACM SIGKDD international conference on Knowledge discovery and data mining*, pages 81–90. ACM, 2000.
- H. Glanz and L. Carvalho. An expectation-maximization algorithm for the matrix normal distribution. *arXiv preprint arXiv:1309.6609*, 2013.
- M. Gönen and E. Alpaydm. Multiple kernel learning algorithms. *Journal of machine learning research*, 12(Jul):2211–2268, 2011.
- M. J. Graham, S. G. Djorgovski, A. A. Mahabal, C. Donalek, and A. J. Drake. Machine-assisted discovery of relationships in astronomy. *MNRAS*, 431: 2371–2384, May 2013a.
- M. J. Graham, A. J. Drake, S. G. Djorgovski, et al. A comparison of period finding algorithms. *MNRAS*, 434:3423–3444, October 2013b.
- A. Gupta and D. Nagar. Matrix variate distributions. monographs and surveys in pure and applied mathematics, 2000.
- R. Haber, A. Rangarajan, and A. M. Peter. Discriminative Interpolation for Classification of Functional Data. In *Joint European Conference on Machine Learning and Knowledge Discovery in Databases*, pages 20–36. Springer, 2015.
- T. Hastie, R. Tibshirani, and J. Friedman. *The elements of statistical learning*, volume 2. Springer, 2009.
- E. Helfer, B. Smith, R. Haber, and A. Peter. Statistical Analysis of Functional Data. Technical report, Florida Institute of Technology, 2015.
- T. A. Hinnert, K. Tat, and R. Thorp. Machine Learning Techniques for Stellar Light Curve Classification. *AJ*, 156:7, July 2018.
- H. Hotelling. Relations between two sets of variates. *Biometrika*, 28(3/4):321–377, 1936.
- J. Hu, J. Lu, J. Yuan, and Y. Tan. Large margin multi-metric learning for face and kinship verification in the wild. In *Asian Conference on Computer Vision*, pages 252–267. Springer, 2014.
- J. Hu, J. Lu, Y. Tan, J. Yuan, and J. Zhou. Local large-margin multi-metric learning for face and kinship verification. *IEEE Transactions on Circuits and Systems for Video Technology*, 28(8):1875–1891, 2018.
- K. E. Iverson. A programming language. In *Proceedings of the May 1-3, 1962, spring joint computer conference*, pages 345–351. ACM, 1962.
- R. A. Johnson, D. W. Wichern, et al. *Applied multivariate statistical analysis*, volume 4. Prentice hall Englewood Cliffs, NJ, 1992.

- K. B. Johnston and H. M. Oluseyi. Generation of a supervised classification algorithm for time-series variable stars with an application to the LINEAR dataset. *New A*, 52:35–47, April 2017. .
- K. B. Johnston and A. M. Peter. Variable Star Signature Classification using Slotted Symbolic Markov Modeling. *New A*, 50:1–11, January 2017. .
- K. B. Johnston, R. Haber, S. M. Caballero-Nieves, A. M. Peter, V. Petit, and M. Knot. A novel detection metric designed for identification of o’connell effect eclipsing binaries. *Computational Astrophysics and Cosmology*, 6(4), 2019. .
- M. Kan, S. Shan, H. Zhang, S. Lao, and X. Chen. Multi-view discriminant analysis. *IEEE transactions on pattern analysis and machine intelligence*, 38(1): 188–194, 2016.
- E. Keogh, X. Xi, L. Wei, and C. A. Ratanamahatana. The ucr time series classification/clustering homepage, 2011.
- D.-W. Kim and C. A. L. Bailer-Jones. A package for the automated classification of periodic variable stars. *A&A*, 587:A18, March 2016. .
- J. Kittler, M. Hatef, R. P. W. Duin, and J. Matas. On combining classifiers. *IEEE transactions on pattern analysis and machine intelligence*, 20(3):226–239, 1998.
- J. Lin, E. Keogh, L. Wei, and S. Lonardi. Experiencing SAX: a novel symbolic representation of time series. *Data Min. Knowl. Discov.*, 15(2):107–144, October 2007. ISSN 1384-5810. . URL <http://dx.doi.org/10.1007/s10618-007-0064-z>.
- A. Mahabal, K. Sheth, F. Gieseke, et al. Deep-learned classification of light curves. In *Computational Intelligence (SSCI), 2017 IEEE Symposium Series on*, pages 1–8. IEEE, 2017.
- F. J. Masci, D. I. Hoffman, C. J. Grillmair, and R. M. Cutri. Automated Classification of Periodic Variable Stars Detected by the Wide-field Infrared Survey Explorer. *AJ*, 148:21, July 2014. .
- P. R. McWhirter, I. A. Steele, D. Al-Jumeily, A. Hussain, and M. M. B. R. Velasco. The classification of periodic light curves from non-survey optimized observational data through automated extraction of phase-based visual features. In *Neural Networks (IJCNN), 2017 International Joint Conference on*, pages 3058–3065. IEEE, 2017.
- A. A. Miller, J. S. Bloom, J. W. Richards, et al. A Machine-learning Method to Infer Fundamental Stellar Parameters from Photometric Light Curves. *ApJ*, 798:122, January 2015. .
- S. Modak, T. Chattopadhyay, and A. K. Chattopadhyay. Unsupervised classification of eclipsing binary light curves through k-medoids clustering. *arXiv e-prints*, January 2018.
- B. Naul, J. S. Bloom, F. Pérez, and S. van der Walt. A recurrent neural network for classification of unevenly sampled variable stars. *Nature Astronomy*, 2: 151–155, November 2018. .
- L. Nørgaard, R. Bro, F. Westad, and S. B. Engelsen. A modification of canonical variates analysis to handle highly collinear multivariate data. *Journal of Chemometrics*, 20(8-10):425–435, 2006.
- I. Nun, P. Protopapas, B. Sim, M. Zhu, et al. FATS: Feature Analysis for Time Series. *arXiv e-prints*, May 2015.
- L. Palaversa, Ž. Ivezić, L. Eyler, et al. Exploring the Variable Sky with LINEAR. III. Classification of Periodic Light Curves. *AJ*, 146:101, October 2013. .
- H. Park, M. Jeon, and J. B. Rosen. Lower dimensional representation of text data based on centroids and least squares. *BIT Numerical mathematics*, 43 (2):427–448, 2003.
- M. J. Park and S. S. Cho. Functional Data Classification of Variable Stars. *CSAM (Communications for Statistical Applications and Methods)*, 20(4):271–281, 2013.
- I. N. Pashchenko, K. V. Sokolovsky, and P. Gavras. Machine learning search for variable stars. *MNRAS*, 475:2326–2343, April 2018. .
- K. B. Petersen, M. S. Pedersen, et al. The matrix cookbook. *Technical University of Denmark*, 7(15):510, 2008.
- P. Protopapas, J. M. Giammarco, L. Faccioli, M. F. Struble, R. Dave, and C. Alcock. Finding outlier light curves in catalogues of periodic variable stars. *MNRAS*, 369:677–696, June 2006. .
- K. Rehfeld, N. Marwan, J. Heitzig, and J. Kurths. Comparison of correlation analysis techniques for irregularly sampled time series. *Nonlinear Processes in Geophysics*, 18(3):389–404, 2011.
- J. D. Reimann. *Frequency Estimation Using Unequally-Spaced Astronomical Data*. PhD thesis, UNIVERSITY OF CALIFORNIA, BERKELEY., January 1994.
- J. D. M. Rennie and N. Srebro. Loss functions for preference levels: Regression with discrete ordered labels. In *Proceedings of the IJCAI multidisciplinary workshop on advances in preference handling*, pages 180–186. Kluwer Norwell, MA, 2005.
- J. W. Richards, D. L. Starr, N. R. Butler, et al. On Machine-learned Classification of Variable Stars with Sparse and Noisy Time-series Data. *ApJ*, 733:10, May 2011. .
- J. W. Richards, D. L. Starr, A. A. Miller, et al. Construction of a Calibrated Probabilistic Classification Catalog: Application to 50k Variable Sources in the All-Sky Automated Survey. *ApJS*, 203:32, December 2012. .
- S. Ruder. An overview of gradient descent optimization algorithms. *arXiv preprint arXiv:1609.04747*, 2016.
- M. Safayani and M. T. M. Shalmani. Matrix-variate probabilistic model for canonical correlation analysis. *EURASIP Journal on Advances in Signal Processing*, 2011(1):748430, 2011.
- N. N. Samus’, E. V. Kazarovets, O. V. Durlевич, et al. General catalogue of variable stars: Version GCVS 5.1. *Astronomy Reports*, 61:80–88, January 2017. .
- M. Scholz. *Approaches to analyse and interpret biological profile data*. PhD thesis, University of Potsdam, Germany, 2006.
- M. Schultz and T. Joachims. Learning a distance metric from relative comparisons. In *Advances in neural information processing systems*, pages 41–48, 2004.
- B. Sesar, J. S. Stuart, Ž. Ivezić, et al. Exploring the Variable Sky with LINEAR. I. Photometric Recalibration with the Sloan Digital Sky Survey. *AJ*, 142:190, December 2011. .
- L. Sevilla-Lara and E. Learned-Miller. Distribution fields for tracking. In *Computer Vision and Pattern Recognition (CVPR), 2012 IEEE Conference on*, pages 1910–1917. IEEE, 2012.
- M. Sokolova and G. Lapalme. A systematic analysis of performance measures for classification tasks. *Information Processing & Management*, 45(4):427–437, 2009.
- D. M. J. Tax. *One-class Classification*. PhD thesis, Delft University of Technology, 2001.
- D. M. J. Tax and K. R. Muller. Feature extraction for one-class classification. In *Proceedings of the ICANN/ICONIP*, pages 342–349, 2003.
- JUnit Team. Junit, 2018a. URL <https://junit.org>.
- MatFileRW Team. Matfilerw. github, 2018b. URL <https://github.com/diffplug/matfilerw>.
- Quality Open Software Team. Simple logging facade for java (slf4j), 2017. URL <https://www.slf4j.org/index.html>.
- L. Torresani and K. Lee. Large margin component analysis. In *Advances in neural information processing systems*, pages 1385–1392, 2007.
- L. Valenzuela and K. Pichara. Unsupervised classification of variable stars. *MNRAS*, 474:3259–3272, March 2018. .
- K. Q. Weinberger, J. Blitzer, and L. K. Saul. Distance metric learning for large margin nearest neighbor classification. *J. Mach. Learn. Res.*, 10:207–244, June 2009. ISSN 1532-4435. URL <http://dl.acm.org/citation.cfm?id=1577069.1577078>.
- H. Wold. A Study in Analysis of Stationary Time Series. *Journal of the Royal Statistical Society*, 102(2):295–298, 1939.
- C. Xu, D. Tao, and C. Xu. A survey on multi-view learning. *arXiv preprint arXiv:1304.5634*, 2013.
- T. Zhang and F. J. Oles. Text categorization based on regularized linear classification methods. *Information retrieval*, 4(1):5–31, 2001.
- L. Zhou, H. Wang, Z. M. Lu, T. Nie, and K. Zhao. Face Recognition Based on LDA and Improved Pairwise-Constrained Multiple Metric Learning Method. *Journal of Information Hiding and Multimedia Signal Processing*, 7(5):1092, 2016.
- S. Zhou et al. Gemini: Graph estimation with matrix variate normal instances. *The Annals of Statistics*, 42(2):532–562, 2014.
- X. Zhu, Z. Huang, H. T. Shen, et al. Dimensionality reduction by mixed kernel canonical correlation analysis. *Pattern Recognition*, 45(8):3003–3016, 2012.

Appendix A: Challenges Addressed

In the application of the LM³L algorithm to our data we found a number of challenges not specified by the original paper that required attention. Some of these challenges were a direct result of our views (vectorization of matrix-variate data) and some of these challenges were resulting from practical application (hinge loss functionality and step-size optimization).

Appendix A.1: Hinge Loss Functionality

While the original LM³L paper does not specify details with respect to the implementation of the hinge loss functionality used, the numerical implementation of both the maxima and the derivative of the maxima are of critical importance. For the implementation here, the hinge-loss functionality is approximated using Generalized Logistic Regression (Zhang and Oles 2001; Rennie and Srebro 2005). Should a different approximation of hinge loss be requested, care should be given to the implementation, as definitions from various public sources are not consistent. For purposes here, the Generalized Logistic Regression is used to approximate the hinge loss ($h[x] \approx g_+(z, \phi)$) and is defined as equation A.1:

$$g_+(z, \phi) = \begin{cases} 0.0 & z \leq -10 \\ z & z \geq 10 \\ \frac{1}{\phi} \log(1 + \exp(z\phi)) & -10 < z < 10 \end{cases} \quad (\text{A.1})$$

the derivative of the Generalized Logistic Regression is then given as equation A.2:

$$\frac{\partial g_+(z, \phi)}{\partial z} = \begin{cases} 0.0 & z \leq -10 \\ 1 & z \geq 10 \\ \frac{\exp(\phi z)}{1 + \exp(\phi z)} & -10 < z < 10 \end{cases} \quad (\text{A.2})$$

For practical reasons (underflow/overflow) the algorithm is presented as a piece-wise function, in particular this is necessary because of the exponential in the functionality. In addition, the public literature is not consistent on the definition of the hinge-loss functionality approximation, specifically the relationship between the notations: $[z]_+$, $h[z]$, $\max(z, 0)$, and $g_+(z, \phi)$; usually the inconsistency is with respect to the input i.e. z , $-z$, or $1 - z$. We have explicitly stated our implementation here to eliminate any confusion.

Appendix A.2: Step-Size Optimization

While LM³L provides an approximate "good" step size to use, in practice we found that a singular number was not necessarily useful. While the exact reasons of why a constant step size was not beneficial were not investigated; the following challenges were identified:

1. The possibility of convergence was very sensitive to the step size.
2. Small step sizes that did result in a consistent optimization, resulted in a very slow convergence.
3. While an attempt could be made to find an optimal step size with respect to all views, it seems unlikely this would occur given the disparate nature of the views we have selected (distribution field, photometric color, time domain statistics, etc.).

4. For the metric learning methods used here (in both the standard and the proposed algorithms) the objective function magnitude scales with the number of training data sets, view dimensions and the number of views, as is apparent from the individual component of LM³L: $\sum_{i,j} h[\tau_k - y_{ij}(\eta_k - d_{\mathbf{M}_k}^2(x_i^k, x_j^k))]$. With increasing number of training data, the objective function will increase and the gradient component ($w_k^p \sum_{i,j} y_{ij} h'[z] \mathbf{C}_{ij}^k$) will similarly be affected. This means that computational overflows could occur just by increasing the number of training data used.

In lieu of a singular estimate, we propose a dynamic estimate of the step-size per iteration per view. A review of step-size and gradient descent optimization methods (Ruder 2016) suggest a number of out-of-the-box solutions to the question of speed (specifically methods such as Mini-Batch gradient descent).

The question of dynamic step size requires more development, in particular while methods exists, these are almost entirely focused on vector variate optimization. Barzilai and Borwein (1988) outline a method for dynamic step size estimation that has its' basis in secant root finding, the method described is extended here to allow for matrix variate cases. The gradient descent update for our metric learning algorithm is given as equation A.3.

$$\mathbf{L}^{(t+1)} = \mathbf{L}^{(t)} - \beta \frac{\partial J}{\partial \mathbf{L}} \quad (\text{A.3})$$

In the spirit of Barzilai and Borwein, here in known as the BB-step method, the descent algorithm is reformulated as equation A.4:

$$\lambda_k = \arg \min_{\lambda} \|\Delta \mathbf{L} - \lambda \Delta g(\mathbf{L})\|_F^2 \quad (\text{A.4})$$

where λ_k is a dynamic step size to be estimated per iteration and per view, $\Delta g(\mathbf{L}) = \nabla f(\mathbf{L}^{(t)}) - \nabla f(\mathbf{L}^{(t-1)})$ and $\Delta \mathbf{L} = \mathbf{L}^{(t)} - \mathbf{L}^{(t-1)}$. The Forbinus norm can be defined as $\|A\|_F^2 = \text{Tr}(A \cdot A^H)$, the BB-step method can be found as equation A.5:

$$\frac{\partial}{\partial \lambda} \text{Tr}[(\Delta \mathbf{L} - \lambda \Delta g(\mathbf{L}))(\Delta \mathbf{L} - \lambda \Delta g(\mathbf{L}))^H] = 0 \quad (\text{A.5})$$

Based on the Matrix Cookbook (Petersen et al. 2008), equation A.5 can be transformed into equation A.6.

$$\text{Tr}[-\Delta g(\mathbf{L})[\Delta \mathbf{L} - \lambda \Delta g(\mathbf{L})]^H - [\Delta \mathbf{L} - \lambda \Delta g(\mathbf{L})]\Delta g(\mathbf{L})^H] = 0 \quad (\text{A.6})$$

With some algebra, equation A.6 is turned into a solution for an approximation of optimal step size, given here as equation A.7.

$$\hat{\lambda} = \frac{1}{2} \cdot \frac{\text{Tr}[\Delta g(\mathbf{L}) \cdot \Delta \mathbf{L}^H + \Delta \mathbf{L} \cdot \Delta g(\mathbf{L})^H]}{\text{Tr}[\Delta g(\mathbf{L}) \cdot \Delta g(\mathbf{L})^H]} \quad (\text{A.7})$$

It is elementary to show that our methodology can be extended for $\Delta g(\mathbf{L}_k) = \nabla f(\mathbf{L}_k^{(t)}) - \nabla f(\mathbf{L}_k^{(t-1)})$ and $\Delta \mathbf{L}_k = \mathbf{L}_k^{(t)} - \mathbf{L}_k^{(t-1)}$; likewise we can estimate $\hat{\lambda}_k$ per view, so long as the estimates of both gradient and objective function are monitored at each iteration. While this addresses our observations, it should

be noted that the fourth challenged outlined (scaling with increasing features and training data) was only partially addressed. Specifically, the above methodology does not address an initial guess of λ_k ; in multiple cases it was found that this initial value was set to high, causing our optimization to diverge. Providing an initial metric in the form of $\sigma\mathbb{I}$ where $0 < \sigma < 1$, was found to improve the chances of success, where the σ was used to offset a J value (from the objective function) that was too high (overflow problems). Care should be taken to set both the initial λ_k and σ to avoid problems.

Appendix A.3: Vectorization and ECVA

The features focused on, as part of our implementation, include both vector variate and matrix variate views. The matrix variate views requires transformation from their matrix domain to a vectorized domain for implementation in the LM³L framework. The matrix-variate to vector-variate transformation implemented here is outlined in Johnston and Peter (2017). The matrix is transformed $\text{vec}(X_i^k) = x_i^k$ to a vector domain. A dimensionality reduction process is implemented as some of the matrices are large enough to result in large sparse vectors (i.e., 20×20 DF matrix = 400 element vector). To reduce the large sparse feature vector resulting from the unpacking of matrix, we applied a supervised dimensionality reduction technique commonly referred to as extended canonical variate analysis (ECVA) (Nørgaard et al. 2006).

The methodology for ECVA has roots in principle component analysis (PCA). PCA is a procedure performed on large multidimensional datasets with the intent of rotating what is a set of possibly correlated dimensions into a set of linearly uncorrelated variables (Scholz 2006). The transformation results in a dataset, where the first principle component (dimension) has the largest possible variance. PCA is an unsupervised methodology—known labels for the data being processed is not taken into consideration—thus a reduction in feature dimensionality will occur. While PCA maximizes the variance, it might not maximize the linear separability of the class space.

In contrast to PCA, Canonical Variate Analysis (CVA) does take class labels into considerations. The variation between groups is maximized resulting in a transformation that benefits the goal of separating classes. Given a set of data \mathbf{x} with: g different classes, n_i observations of each class; following Johnson et al. (1992), the within-group and between-group covariance matrix is defined as equations A.8 and A.9 respectively.

$$\mathbf{S}_{\text{within}} = \frac{1}{n-g} \sum_{i=1}^g \sum_{j=1}^{n_i} (x_{ij} - \bar{x}_{ij})(x_{ij} - \bar{x}_{ij})' \quad (\text{A.8})$$

$$\mathbf{S}_{\text{between}} = \frac{1}{g-1} \sum_{i=1}^g n_i (x_i - \bar{x})(x_i - \bar{x})' \quad (\text{A.9})$$

Where $n = \sum_{i=1}^g n_i$, $\bar{x}_i = \frac{1}{n_i} \sum_{j=1}^{n_i} x_{ij}$, and $\bar{x} = \frac{1}{n} \sum_{j=1}^{n_i} n_i x_i$. CVA attempts to maximize the equation A.10.

$$J(\mathbf{w}) = \frac{\mathbf{w}' \mathbf{S}_{\text{between}} \mathbf{w}}{\mathbf{w}' \mathbf{S}_{\text{within}} \mathbf{w}} \quad (\text{A.10})$$

The equation is solvable so long as $\mathbf{S}_{\text{within}}$ is non-singular, which need not be the case, especially when analyzing multicollinear data. When the case arises that the dimensions of the

observed patterns are multicollinear, additional considerations need to be made. Nørgaard et al. (2006) outlines a methodology, Extended Canonical Variate Analysis (ECVA), for handling these cases in CVA. Partial least squares analysis (PLS2, Wold 1939) is used to solve the above linear equation, resulting in an estimate of \mathbf{w} , and given that, an estimate of the canonical variates (the reduced dimension set). The application of ECVA to our vectorized matrices results in a reduced feature space of dimension $g-1$, this reduced dimensional feature space, per view, is then used in the LM³L classifier.

Appendix B: Derivation of Large Margin Multi-View Metric Learning with Matrix Variates

This objective design is solved using a gradient descent solver operation. To enforce the requirements of $\mathbf{U}_k > 0$ and $\mathbf{V}_k > 0$, the metrics are decomposed— $\mathbf{U}_k = \mathbf{\Gamma}_k^T \mathbf{\Gamma}_k$ and $\mathbf{V}_k = \mathbf{N}_k^T \mathbf{N}_k$. The gradient of the objective function with respect to the decomposed matrices $\mathbf{\Gamma}_k$ and \mathbf{N}_k is estimated. The unconstrained optimum is found using the gradient of the decomposed matrices; the \mathbf{U}_k and \mathbf{V}_k matrices are then reconstituted at the end of the optimization process. We reformulate the matrix variate distance as equation B.1:

$$d_{\mathbf{\Gamma}_k, \mathbf{N}_k}(\Delta_{ij}^k) = \text{tr} \left[\mathbf{\Gamma}_k^T \mathbf{\Gamma}_k (\Delta_{ij}^k)^T \mathbf{N}_k^T \mathbf{N}_k (\Delta_{ij}^k) \right]; \quad (\text{B.1})$$

for ease we make the following additional definitions: $d_{\mathbf{U}_k, \mathbf{V}_k}(X_i^k, X_j^k) = d_{ij}^k$, $X_i^k - X_j^k = \Delta_{ij}^k$, $\mathbf{A}_{ij}^k = (\Delta_{ij}^k)^T \mathbf{N}_k^T \mathbf{N}_k (\Delta_{ij}^k)$, and $\mathbf{B}_{ij}^k = \Delta_{ij}^k \mathbf{\Gamma}_k^T \mathbf{\Gamma}_k (\Delta_{ij}^k)^T$. Note that $\mathbf{A}_{ij}^k = (\mathbf{A}_{ij}^k)^T$ and $\mathbf{B}_{ij}^k = (\mathbf{B}_{ij}^k)^T$. Additionally we identify the gradients as equations B.2 and B.3:

$$2\mathbf{\Gamma}_k \mathbf{A}_{ij}^k = \frac{\partial d_{ij}^k}{\partial \mathbf{\Gamma}_k} \quad (\text{B.2})$$

$$2\mathbf{N}_k \mathbf{B}_{ij}^k = \frac{\partial d_{ij}^k}{\partial \mathbf{N}_k}, \quad (\text{B.3})$$

as being pertinent for derivation. We give the gradient of the individual view objective I_k as equations B.4 and B.5:

$$\frac{\partial I_k}{\partial \mathbf{\Gamma}_k} = 2\mathbf{\Gamma}_k \left((1-\gamma) \sum_{i,j} \eta_{ij}^k \cdot \mathbf{A}_{ij}^k + \gamma \sum_{j \rightsquigarrow i,l} \eta_{ij}^k (1-y_{il}) \cdot h'[z] \cdot [\mathbf{A}_{ij}^k - \mathbf{A}_{il}^k] + \lambda \mathbf{I} \right) \quad (\text{B.4})$$

$$\frac{\partial I_k}{\partial \mathbf{N}_k} = 2\mathbf{N}_k \left((1-\gamma) \sum_{i,j} \eta_{ij}^k \cdot \mathbf{B}_{ij}^k + \gamma \sum_{j \rightsquigarrow i,l} \eta_{ij}^k (1-y_{il}) \cdot h'[z] \cdot [\mathbf{B}_{ij}^k - \mathbf{B}_{il}^k] + \lambda \mathbf{I} \right), \quad (\text{B.5})$$

and the gradient of the joint objective as equations B.6 and B.7:

$$\frac{\partial J_k}{\partial \mathbf{\Gamma}_k} = w_k^p \frac{\partial I_k}{\partial \mathbf{\Gamma}_k} + 4\mu \mathbf{\Gamma}_k \sum_{q=1, q \neq k}^K \sum_{i,j} (d_{ij}^k - d_{ij}^q) \mathbf{A}_{ij}^k \quad (\text{B.6})$$

$$\frac{\partial J_k}{\partial \mathbf{N}_k} = w_k^p \frac{\partial I_k}{\partial \mathbf{N}_k} + 4\mu \mathbf{N}_k \sum_{q=1, q \neq k}^K \sum_{i,j} (d_{ij}^k - d_{ij}^q) \mathbf{B}_{ij}^k. \quad (\text{B.7})$$

To estimate the update for the weights, we solve for the Lagrange function given equation B.8:

$$La(w, \eta) = \sum_{k=1}^K w_k^p I_k + \lambda \sum_{k,l=1, k < l}^K \sum_{i,j} (d_{ij}^k - d_{ij}^l)^2 - \eta \left(\sum_{k=1}^K w_k - 1 \right); \quad (\text{B.8})$$

we estimate the weights as equation B.9:

$$w_k = \frac{(1/I_k)^{1/(p-1)}}{\sum_{k=1}^K (1/I_k)^{1/(p-1)}}. \quad (\text{B.9})$$

The implementation of distance in the multi-view case, i.e. implementation of distance used in the k-NN algorithm, is given as equation B.10:

$$d(X_i, X_j) = \sum_{k=1}^K w_k \text{tr} \left[\mathbf{U}_k (X_i^k - X_j^k)^T \mathbf{V}_k (X_i^k - X_j^k) \right] \quad (\text{B.10})$$

We note the following about the algorithm:

1. Similar to LM³L we optimize in two stages at each iteration: freezing the weights and optimizing $\mathbf{\Gamma}_k$ and \mathbf{N}_k with respect to the primary objective function, then freezing the estimates of $\mathbf{\Gamma}_k$ and \mathbf{N}_k and optimizing w_k given the Lagrangian
2. The generation of the gradient for the objective is $\nabla J_k(X_i^k; \mathbf{U}_k, \mathbf{V}_k) = \left[\frac{\partial J_k}{\partial \mathbf{\Gamma}_k}, \frac{\partial J_k}{\partial \mathbf{N}_k} \right]$; simultaneous estimate of the gradient is possible—there no need for flip-flopping the order of operation unlike the estimate of the sample covariance matrices themselves as shown in Glanz and Carvalho (2013).
3. The step sizes for each iteration are estimated using our BB method generated, step sizes for \mathbf{U}_k and \mathbf{V}_k are found independently from each other and from each view, i.e. the equations B.11 and B.12

$$\hat{\beta}_k = \frac{1}{2} \cdot \frac{\text{Tr} [\Delta g(\mathbf{\Gamma}_k) \cdot \Delta \mathbf{\Gamma}_k^H + \Delta \mathbf{\Gamma}_k \cdot \Delta g(\mathbf{\Gamma}_k)^H]}{\text{Tr} [\Delta g(\mathbf{\Gamma}_k) \cdot \Delta g(\mathbf{\Gamma}_k)^H]} \quad (\text{B.11})$$

$$\hat{\kappa}_k = \frac{1}{2} \cdot \frac{\text{Tr} [\Delta g(\mathbf{N}_k) \cdot \Delta \mathbf{N}_k^H + \Delta \mathbf{N}_k \cdot \Delta g(\mathbf{N}_k)^H]}{\text{Tr} [\Delta g(\mathbf{N}_k) \cdot \Delta g(\mathbf{N}_k)^H]} \quad (\text{B.12})$$

The algorithm recombines the decomposed matrices to produce the results $\mathbf{U}_k = \mathbf{\Gamma}_k^T \mathbf{\Gamma}_k$ and $\mathbf{V}_k = \mathbf{N}_k^T \mathbf{N}_k$ per view.

Appendix C: Performance Comparison

Tables C.1 and C.2 contain delta values (differences) of LM³L-MV - LM³L confusion matrices for the datasets analyzed for this paper.

Table C.1. Difference LINEAR confusion matrix, LM³L-MV - LM³L

Misclassification Rate	RR Lyr (ab)	Delta Scu / SX Phe	Algol	RR Lyr (c)	Contact Binary	Missed
RR Lyr (ab)	-7	0	1	9	-1	-2
Delta Scu / SX Phe	1	1	0	0	-2	0
Algol	2	0	-4	1	1	0
RR Lyr (c)	-1	0	0	2	-1	0
Contact Binary	0	0	2	-8	5	1

Table C.2. Difference UCR confusion matrix, LM³L-MV - LM³L

Misclassification Rate	2	3	1	Missed
2	2	-3	0	1
3	-13	-171	184	0
1	-5	92	-87	0